This is a submitted manuscript of the following conference paper: Manayil Santhosh, B & Lappa, M 2025, Morphological evolution of particle accumulation structures induced by thermo-vibrational effects in non-uniformly heated systems under microgravity conditions. in AIAA SCITECH 2025 Forum: 6-10 January 2025, Orlando, FL., AIAA 2025-1698, AIAA American Institute of Aeronautics and Astronautics, Reston, VA.
https://doi.org/10.2514/6.2025-1698

Morphological evolution of Particle Accumulation Structures induced by thermo-vibrational effects in non-uniformly heated systems under microgravity conditions

Balagopal Manayil Santhosh [1] and Marcello Lappa[1*]

[1] PhD Student [1*] Professor(full)

[1,1*]Department of Mechanical and Aerospace Engineering, University of Strathclyde, James Weir Building, 75 Montrose Street, Glasgow, G1 1XJ, UK

Abstract: *With the recent discovery of solid particle attractors in thermo-vibrational flow driven by the interplay of inertial and convective effects in a constrained 3D physical space (as confirmed by dedicated experiments conducted on board the International Space Station), a need has emerged for additional numerical studies aimed at acquiring additional data to improve our understanding of these phenomena and their evolution in the space of parameters. The thermal configuration considered in this study is more complex than that used for the space experiments and consists of two differentially heated opposite walls containing central square patches that are of opposite temperatures (i.e. a cold spot located at the center of the hot wall and vice versa). The driving force is represented by periodic vibrations of specific frequencies, which are applied in such a way that they are perpendicular to the gradients of temperature established between the thermal features pertaining to different boundaries. Two different types of particle structures were reported in a recent study published by the same authors for similar boundary conditions; namely, tubular formations such as those revealed by the space experiments (where no thermal patches were present, i.e. there was a uniformly cooled wall located in front of a uniformly heated wall) and a previously unseen quadrupolar set of structures aligned along a direction perpendicular to such tubular formations. The present study takes it further ahead by increasing the range of considered values of the Rayleigh number to assess the effect of the magnitude of the thermo-vibrational flow field on the morphology and co-existence of these structures. The characteristic numbers, Prandtl number, angular frequency, particle Stokes number and particle-fluid density ratio are fixed at 6.11 (water at ambient temperature), $\omega=10^3$, $St= 5\times10^{-6}$ and $\xi=2$ respectively whereas the vibrational Rayleigh number spans the interval $5\times10^3< Ra_\omega <10^5$. It is shown that when the Rayleigh number is increased, the quadrupolar formation, which previously was a secondary effect (having a limited spatial extension) becomes so dominant that the tubular formations cease to exist.*

Keywords: *Particle dynamics, vibrational flow, numerical simulation, Eulerian-Lagrangian approach*

Nomenclature:

α	*Fluid thermal diffusivity*
β_T	*Fluid thermal expansion coefficient*
ω	*Angular frequency*
ρ	*Fluid density*
$g(t)$	*Time varying acceleration*
b	*Amplitude(m)*
f	*Frequency in hertz*
L	*Characteristic length*
γ	*Non-dimensional acceleration amplitude*
ξ	*Particle to fluid density ratio*
ϕ	*Angle of incidence of vibrations*
l_s	*Thermal spot size*
Ω	*Non-dimensional angular frequency of vibrations*
Pr	*Prandtl number*
t	*Non-dimensional time*
P	*Non-dimensional period of vibrations.*
μ	*Dynamic viscosity*
Ra_ω	*Vibrational Rayleigh number*
St	*Particle Stokes number*

1. Introduction

Multiphase systems such as suspensions, emulsions, foams, and wet granular media, consisting of a dispersed minority phase into a majority phase, exhibit a variety of behaviors depending on the interactions between such constitutive phases. Such phenomena are of a great scientific and technological interest owing to their pervasive presence in Nature and involvement in a number of industrial applications [1-6]. Moreover, they can cover a wide range of scales, from micrometers to several meters [7]. In such a context, the present study focuses on a recent avenue, namely, designing solid particle management technologies in fluid flow by harnessing the inertial properties of the dispersed phase. More precisely, this research should be regarded as an extension of the same author's work on a particular thermal configuration that yielded interesting phenomena under the effect of externally imposed vibrations in a reduced gravity environment [8].

For the convenience of the reader, in the following the characteristics of the peculiar type of flow induced by vibrations are introduced along with a brief explanation of the solid particle self-organization phenomena, which occur in a dilute fluid medium. Dense particle-fluid systems are not considered here as they exhibit intriguing behaviors influenced by particle-particle interactions that are complicated and will be examined in future studies [9]. Vice versa, the self-organization of inertial particles in dilute vibrated fluid-particle systems is well-understood and backed by previous research from various research groups [10,11] (including present authors' work [8]).

Here we consider the typical situation where: 1) solid particles, due to their inertial properties, develop an independent velocity field with respect to the incompressible carrier fluid flow, which allows separation and accumulation in specific sub-regions of the fluid container; 2) the carrier flow's topology remains influential, with closed paths or repetitive (time periodic) behaviors acting as attracting loci for particle concentration [12-13]; 3) gravity is absent (microgravity conditions). Put simply, we explore a scenario where vibrations applied to a non-isothermal fluid induce time-periodic (thermo-vibrational) convection, resulting in inertial particle structures. As a distinguishing mark with respect to other phenomena where inertial particles are involved, in this case these structures display extreme regularity and three-dimensional shapes mimicking quadric surfaces of projective geometry. It is also worth recalling that thermo-vibrational convection is a variant of the buoyancy driven natural convection found in numerous natural phenomena [14-18].

Existing research has extensively described these geometrical structures, resembling ellipsoids, paraboloids, hyperboloids, and cylindrical and conical surfaces in a differentially heated cubic cavity (with one hot wall, an opposing cold wall and the other walls assumed to be adiabatic) and vibrations in different directions. The findings, have been obtained through numerical studies and experiments on board the International Space Station [19]: However, more recent studies have concentrated on more complex thermal configurations in order to explore the possibility to modulate or tune precisely the morphology of the structures emerging in the bulk of the fluid through modification of the temperature boundary conditions on the "surface" of the related container. In such a way, the existence of new types of structures has been discovered. It has been shown numerically that if the otherwise uniform hot and cold walls are perturbed by central spots of opposite temperature, two types of structures can coexist [8]. In turn, this leads to an increase in the multiplicity of structures, i.e. their overall number. This study takes it further by exploring these particular cases by increasing the intensity of the driving force, i.e. the so-called 'vibrational Rayleigh number'. The present investigation addresses this gap by studying fully three-dimensional cases under the influence of a multi-directional temperature gradient and incorporating changes in the above-mentioned vibrational Rayleigh number.

The paper conclusively discusses the importance of varying these parameters to develop a framework that contributes to identifying general principles governing vibrationally driven particle self-organization phenomena in systems with complex thermal configurations.

2. Mathematical Model and Methods

2.1 Geometric and Thermal Boundary Conditions

This investigation revisits the standard cubic cavity initially examined by [14-18,20] As outlined in the introduction, the recent discovery of new morphologies in particle structures and changes in the multiplicity of attracting loci [21] paved the way for exploring the effect of thermally inhomogeneous boundary conditions introduced as patches on the surface of a cubic space (see Figure 1). A key focus here is the generalization of findings related to two-dimensional (2D) configurations to a fully three-dimensional (3D) space and an extension of the range of the vibrational Rayleigh number examined in earlier numerical studies [8].

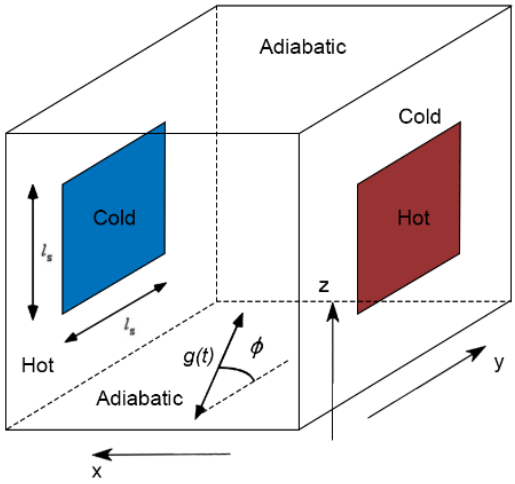

Figure 1: *Sketch of the considered thermal boundary conditions: two thermally controlled opposing walls are set at a temperature T_{cold} and T_{hot}, respectively; each wall, however, is featured by a centrally located square spot having the same temperature of the opposing wall*

2.2 Driving force and governing equations for the fluid phase

Elaborate descriptions and discussions of the forces involved in the considered problem have been delineated in previous research carried out by [14-18,22]and for this reason, they are not duplicated here. In this section, we limit ourselves to recalling that vibrations can be mathematically modeled as a sinusoidal displacement along a direction $\underline{\hat{n}}$, varying with time, defined by an amplitude b (m) and an angular frequency ω rad/s where $\omega=2\pi f$ and f is the frequency in hertz. From a dynamic point of view, this is equivalent to considering a time varying acceleration g(t) with the same period of vibrations and a magnitude which is given by b times the square of ω, i.e. $b\omega^2$. The Boussinesq approximation valid for liquids can be used to directly integrate this dynamic effect into the momentum balance equation. The driving force for fluid flow, therefore, reduces to a source term ρg(t) in the momentum equation where the fluid density ρ is replaced by a corresponding linear function of the fluid temperature.
In this framework, the governing mass, momentum and energy equations for the fluid phase can therefore be cast in compact non-dimensional form, respectively, as

$$\underline{\nabla}\cdot\underline{V}=0 \tag{1}$$

$$\frac{\partial \underline{V}}{\partial t}=-\underline{\nabla}p-\underline{\nabla}\cdot\left[\underline{V}\underline{V}\right]+\mathrm{Pr}\,\nabla^2\underline{V}-\mathrm{Pr}\,Ra_{\omega}T\sin(\Omega t)\underline{\hat{n}} \tag{2}$$

$$\frac{\partial T}{\partial t}+\underline{\nabla}\cdot\left[\underline{V}T\right]=\nabla^2 T \tag{3}$$

where $\underline{V}$, p and T are the non-dimensional velocity (with components u, v and w along x, y and z, respectively), pressure and temperature. In doing so we have implicitly assumed that the reference quantities for all lengths, the velocity, the time, the pressure and the temperature are the size of the cavity (L), (α/L), (L^2/α), ($\rho\alpha^2/L^2$) and $\Delta T= T_{hot}-T_{cold}$, respectively, where L is the cubic cavity side length and α is the fluid thermal diffusivity. The characteristic numbers appearing in these equations represent effective degrees of freedom of the considered system in terms of possible fluid-dynamic behaviors. These are

$$\mathrm{Pr}=\frac{\nu}{\alpha} \tag{4}$$

i.e. the well-known Prandtl number, (where ν is the fluid kinematic viscosity given by the ratio of dynamic viscosity and fluid density, i.e., $\nu=\mu/\rho$ and α is the aforementioned fluid thermal diffusivity). Moreover, Ra_ω appearing in the buoyancy term is the vibrational Rayleigh number, analogue to the classical Rayleigh number used in standard gravitational convection problems (Ra), namely:

$$Ra_\omega=\frac{(b\omega^2\beta_T\Delta T L^3)}{\nu\alpha} \tag{5}$$

where β_T is the fluid thermal expansion coefficient. Lastly, Ω is the non-dimensional angular frequency of the vibrations defined as:

$$\Omega=\frac{\omega L^2}{\alpha}=\frac{2\pi}{P} \tag{6}$$

where P is the non-dimensional period of vibrations.

2.3 Driving force and governing equations for the solid/particulate phase

In line with the majority of research on this specific subject, which has been based on a model that describes the fluid behavior using classical fluid mechanics, i.e. the aforementioned Navier-Stokes equations (1)-(3) and the particle dynamics in the framework of a segregated (but properly coupled) Lagrangian approach, here we resort to a one-way coupled strategy [13-16]. This means that solid particles do not influence the carrier flow and are used solely to reveal the properties of the underlying attractors, which in this case behave as undisturbed templates for the accumulation of particles (the ability of the dispersed mass to induce asymmetries and other effects in the otherwise undisturbed flow has already been explored in an earlier work, to which the interested reader is referred, [20].

The transport equation for the solid particles, accordingly reads:

$$\frac{d\underline{V}_p}{dt}=\frac{1}{\xi+1/2}\left[-\frac{\mathrm{Pr}}{St}f(\mathrm{Re}_p)\left(\underline{V}_p-\underline{V}\right)+\frac{3}{2}\frac{d\underline{V}}{dt}+\frac{3}{2}\left(\underline{V}\cdot\underline{\nabla V}\right)\right]+\frac{\xi-1}{\xi+1/2}\gamma\sin(\Omega t)\hat{\underline{n}} \tag{7}$$

where the additional non-dimensional parameter γ reads:

$$\gamma=\frac{b\omega^2 L^3}{\alpha^2} \tag{8}$$

and it accounts for the non-dimensional amplitude of the acceleration induced by vibrations. Moreover, $\underline{V}_p=[u_p, v_p, w_p]$ is the particle velocity and Re_p is the related instantaneous Reynolds number, defined as

$$\mathrm{Re}_p = \frac{2R_p \rho \left| \underline{V} - \underline{V}_p \right|}{\mu} \tag{9}$$

where $f(\mathrm{Re_p})$ is a corrective factor required to account for the departure of the drag from the classical Stokes law [23]:

$$f\left(\mathrm{Re}_p\right) = 1 + 0.15\,\mathrm{Re}_p^{\,0.687} \tag{10}$$

Moreover, the particle to fluid density ratio ξ and the Stokes number St appearing in this equation read:

$$\xi = \rho_P / \rho \tag{11}$$

$$St = \frac{2}{9}\frac{R_P^2}{L^2} \tag{12}$$

where R_p is the particle radius.

2.4 Boundary conditions

The boundary conditions for the solid walls read (refer again to Figure 1):

$\partial T/\partial y = 0$ and $\underline{V} = 0$ for y = 0, y = 1, $0 \le x \le 1$, $0 \le z \le 1$ and $t \ge 0$ (13)

$\partial T/\partial z = 0$ and $\underline{V} = 0$ for z = 0, z = 1, $0 \le x \le 1$, $0 \le y \le 1$ and $t \ge 0$ (14)

$T = 0$ and $\underline{V} = 0$ for x=0, $0 \le y \le 1$, $0 \le z \le ½(1- l_s)$ and $t \ge 0$ (15a)

$T = 0$ and $\underline{V} = 0$ for x=0, $0 \le y \le ½(1- l_s)$, $½(1- l_s) \le z \le ½(1+ l_s)$ and $t \ge 0$ (15b)

$T = 0$ and $\underline{V} = 0$ for x=0, $½(1+ l_s) \le y \le 1$, $½(1- l_s) \le z \le ½(1+ l_s)$ and $t \ge 0$ (15c)

$T = 0$ and $\underline{V} = 0$ for x=0, $0 \le y \le 1$, $½(1+ l_s) \le z \le 1$ and $t \ge 0$ (15d)

$T = 1$ and $\underline{V} = 0$ for x=0, $½(1- l_s) \le y \le ½(1+ l_s)$, $½(1- l_s) \le z \le ½(1+ l_s)$ and $t \ge 0$ (15e)

$T = 1$ and $\underline{V} = 0$ for x=1, $0 \le y \le 1$, $0 \le z \le ½(1- l_s)$ and $t \ge 0$ (16a)

$T = 1$ and $\underline{V} = 0$ for x=1, $0 \le y \le ½(1- l_s)$, $½(1- l_s) \le z \le ½(1+ l_s)$ and $t \ge 0$ (16b)

$T = 1$ and $\underline{V} = 0$ for x=1, $½(1+ l_s) \le y \le 1$, $½(1- l_s) \le z \le ½(1+ l_s)$ and $t \ge 0$ (16c)

$T = 1$ and $\underline{V} = 0$ for x=1, $0 \le y \le 1$, $½(1+ l_s) \le z \le 1$ and $t \ge 0$ (16d)

$T = 0$ and $\underline{V} = 0$ for x=1, $½(1- l_s) \le y \le ½(1+ l_s)$, $½(1- l_s) \le z \le ½(1+ l_s)$ and $t \ge 0$ (16e)

3. The Numerical Method

The numerical problem was formulated and solved in a multistage form. In practice, this corresponds to the well-known projection (pressure-based) method for incompressible fluid flow where an alternate set of equations is integrated in time (equivalent to the original set of mass and momentum balance equations from a mathematical point of view, but not from a numerical standpoint, [24]) in order to obtain a velocity field that satisfies at the same time the incompressibility constraint and the momentum equation. This category of numerical methods stems from physical and mathematical principles involving well-posedness theory, which are key to the physically consistent and computationally reliable method derivation (see,e .g., [25] From a purely practical standpoint, they lead to a procedure articulated into 3 fundamental steps or stages of calculation.

In step 1, the momentum equation is initially integrated in a simplified (unphysical) form where the pressure (gradient) term is not included in order to allow for a straightforward derivation of a new velocity field as a function of the related value known at the earlier time instant. This is achieved considering the following equation:

$$\frac{\partial \underline{V}^*}{\partial t} = \left[-\underline{\nabla} \cdot \left[\underline{V}\underline{V} \right] + \mathrm{Pr}\, \nabla^2 \underline{V} - \mathrm{Pr}\, Ra_\omega T \sin(\Omega t) \underline{\hat{n}} \right] \tag{17}$$

where the first, the second and third term on the right-hand side represent the convective transport, diffusive transport and production of momentum, respectively (but the pressure term is not present, as explained before).

The physical significance of the velocity is then recovered by reintroducing the previously dropped pressure term, which leads to a correction equation, formally expressed as

$$\underline{V} = \underline{V}^* - \Delta t\, \underline{\nabla} p \tag{18}$$

Substitution of this corrected formula into the mass balance equation, i.e. eq. (1), provides another equation effectively needed for the execution of the second stage of calculation, namely, the so-called pressure equation, which, with simple mathematical manipulations, can be cast in compact form as:

$$\nabla^2 p = \frac{1}{\Delta t} \underline{\nabla} \cdot \underline{V}^* \tag{19}$$

Equations (17) and (19) are parabolic and elliptic in nature, respectively. Equation (18) formally closes the numerical problem by allowing the calculation of the final (physically consistent) velocity (after the intermediate velocity $\underline{V}^*$ and p have been determined), thereby playing the role of stage 3 in the overall computational procedure.

The fluid velocity obtained in such a way is used to determine the term appearing at the right-hand side of eq. (7) that accounts for the forces exerted by the fluid on the solid particle. These must be evaluated at the position instantaneously occupied by the particle, thereby introducing the need for relevant interpolation schemes. In the present case, simple linear interpolations have been used. The particle-tracking Lagrangian equation (7) has been integrated for each particle using a 5^{th}-order accurate Runge-Kutta algorithm.

Particle-domain boundary interaction has been implemented by forcing particles to slip along the solid walls, i.e. by setting their radius as the minimal “allowed” distance of their center from the wall itself.

As already explained at the beginning of Sect. 2.3, the strategy illustrated in this section corresponds to a one-way coupling philosophy, that is, the relatively high number of particles used to produce the results reported in Sect. 4 only served to reveal the intricate details of the particle attractors, the effective number of particles being irrelevant, i.e. having no impact on the emerging dynamics. For each 3D simulation, 6.4×10^4 particles have been tracked.

4. Results and Discussions

4.1 Spot Size 0.5

In the following l_s is used to denote the thermal spot size, i.e. the length of the side of the central thermal spot perturbing the otherwise uniform temperature on the opposing thermally controlled walls. Moreover, we refer to earlier results presented in [8]) to highlight the changes occurring when the vibrational Rayleigh number is increased to larger values (present study),

According to earlier numerical results (see Figure 2) for l_s=0.5 and Ra_ω=1×10^4, the particle structures manifest as two distinct categories initially with a total multiplicity of 8; namely, four axially elongated structures oriented along the z axis and a quadrupolar pattern emerging in proximity to the x=1 plane consisting of four shallow cylindrical structures with axes parallel to the x direction.

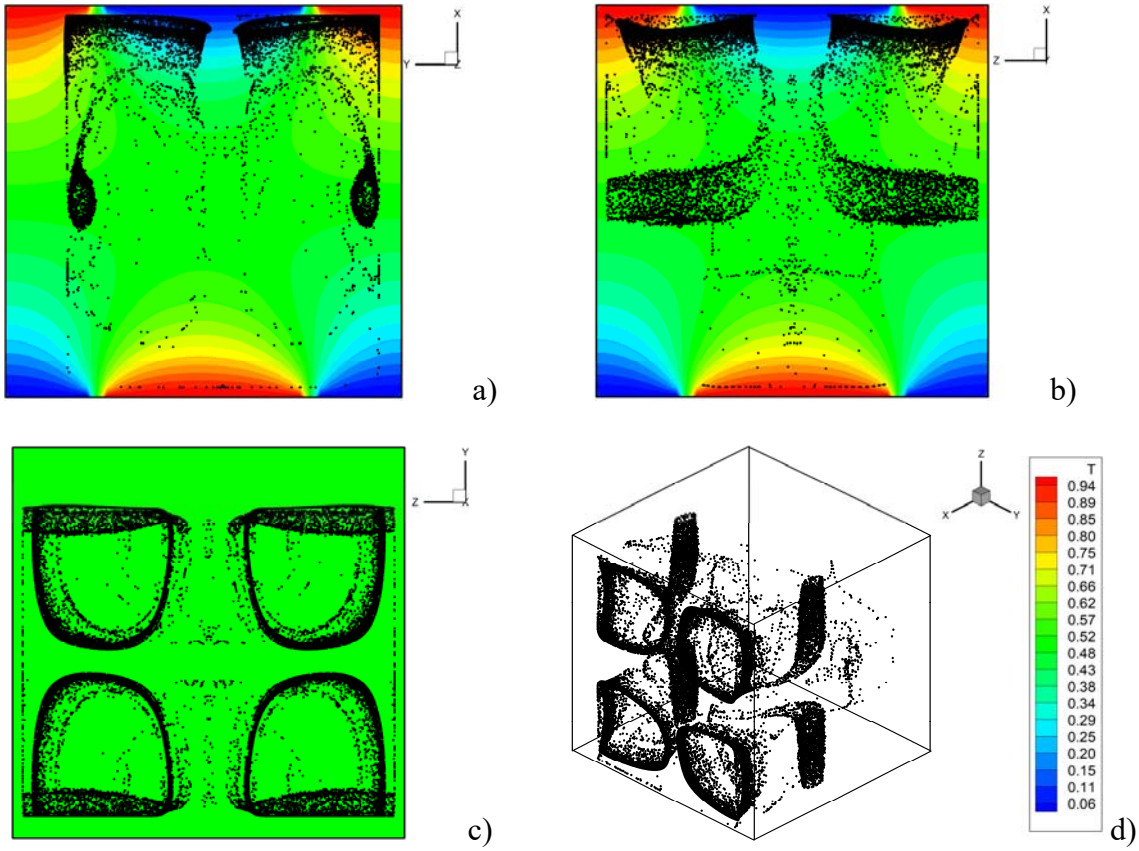

Figure 2: *Snapshot (3D views for t≅8.96) of particle structures and related temperature distribution for γ=10^8, Ra_ω=1×10^4, ϖ=10^3, St=5×10^{-6}, ξ=2, ϕ=0° and l_s=0.5: a) perspective perpendicular to the xy mid-plane, b) perspective perpendicular to the xz mid-plane, c) perspective perpendicular to the yz plane, d) Isometric 3D view.*

Figure 3 clearly indicates that when the Rayleigh number is increased to $Ra_\omega=3\times10^4$, while keeping all the other conditions unchanged, the thickness of the shallow cylindrical formations is reduced drastically. Notably, they exist in the fluid space as narrowed band-like formations compared to the formations seen for $Ra_\omega=1\times10^4$ (Figure 3). As a result, the related quadrupolar pattern is strongly compressed in the +x direction, with the dimensions in the zy plane remaining approximately the same (refer to Figure 3). The most remarkable change, however, relates to the elongated structures with axes oriented along the z direction. Although they are still present, they are barely visible.

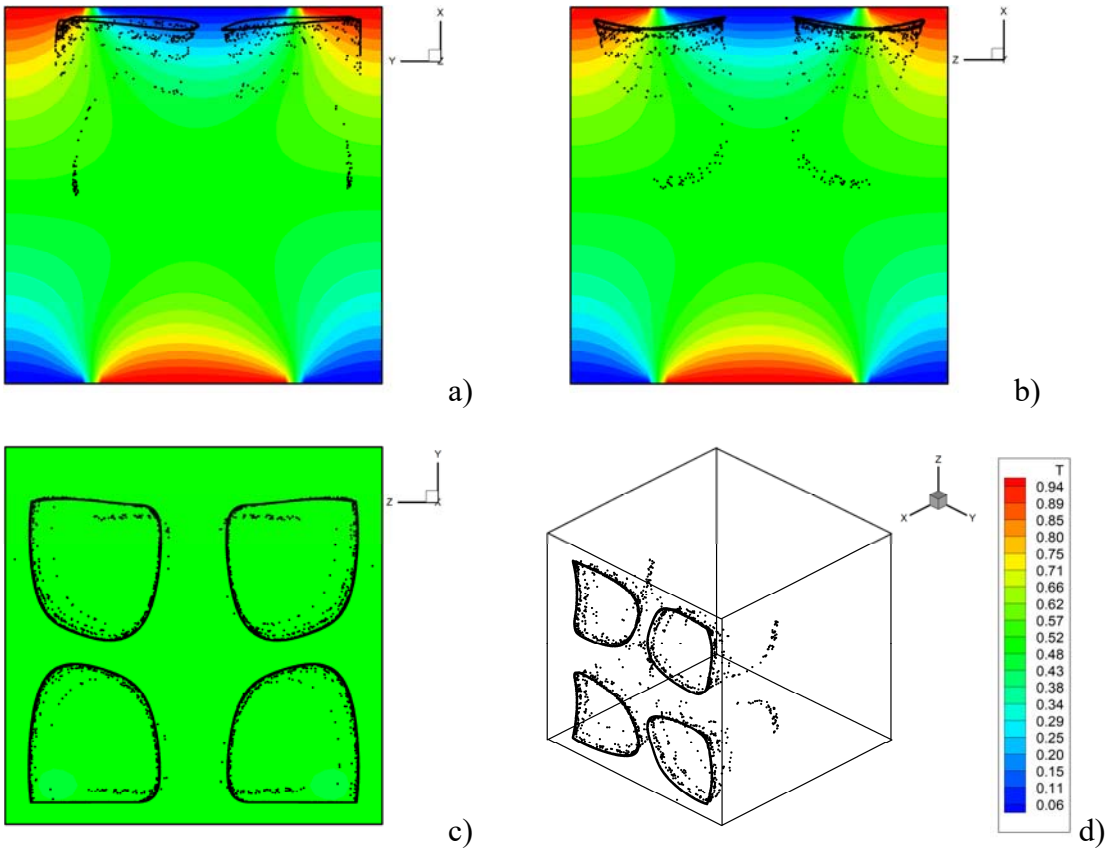

Figure 3: *Snapshot (3D views for t≅8.96) of particle structures and related temperature distribution for $\gamma=10^8$, $Ra_\omega=3\times10^4$, $\varpi=10^3$, $St=5\times10^{-6}$, $\xi=2$, $\phi=0°$ and $l_s=0.5$: a) perspective perpendicular to the xy mid-plane, b) perspective perpendicular to the xz mid-plane, c) perspective perpendicular to the yz plane, d) Isometric 3D view*

Most remarkably, on increasing the vibrational Rayleigh number even more ($Ra_\omega=4\times10^4$ in Figure 4), the elongated formation aligned with the z axis cease to exist. This observation also applies to the case $Ra_\omega=5\times10^4$ (not shown).

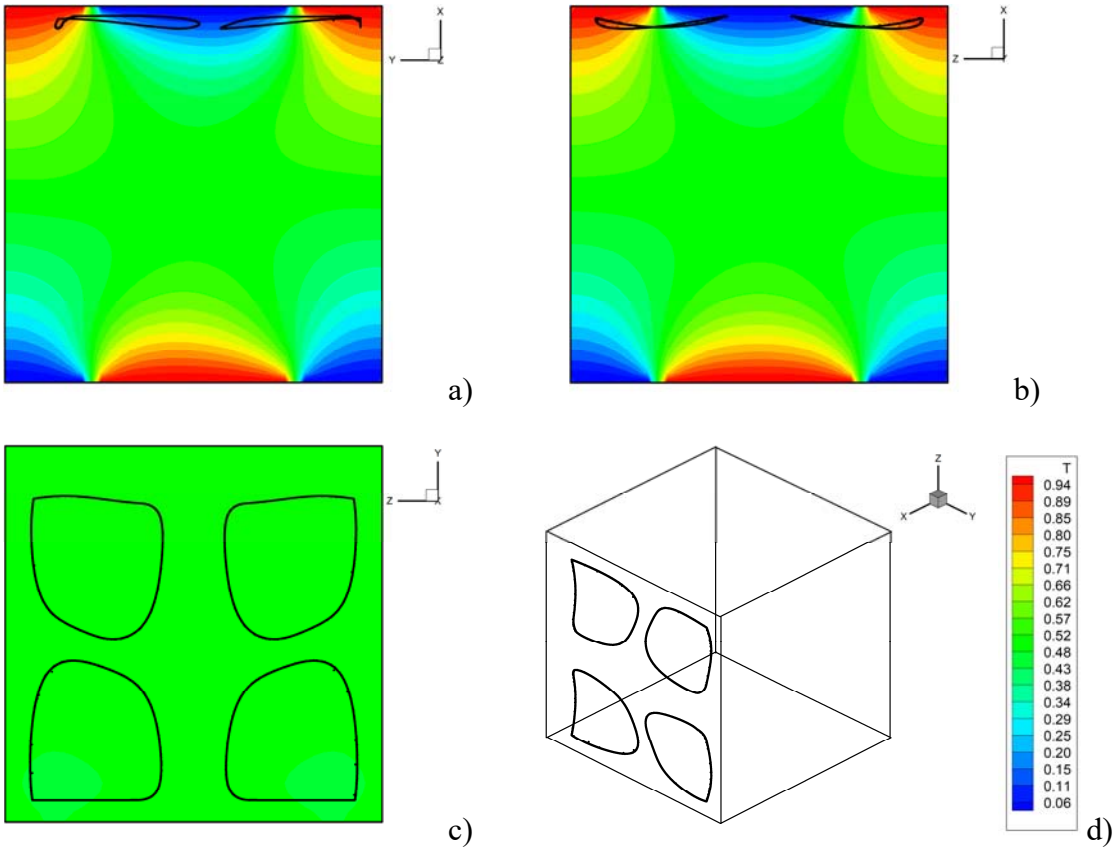

Figure 4: *Snapshot (3D views for t≅8.96) of particle structures and related temperature distribution for $\gamma=10^8$, $Ra_\omega=4\times10^4$, $\varpi=10^3$, $St=5\times10^{-6}$, $\xi=2$, $\phi=0°$ and $l_s=0.5$: a) perspective perpendicular to the xy mid-plane, b) perspective perpendicular to the xz mid-plane, c) perspective perpendicular to the yz plane, d) Isometric 3D view.*

4.2 Spot Size 0.2

To maintain consistency and for ease of comparison with the earlier work, we also consider the case l_s =0.2 for which the previous study [8] only assumed $Ra_\omega=1\times10^4$.
Figure 5 shows that for a slightly smaller value of the vibrational Rayleigh number, the morphology of the structures is essentially the same. More specifically, for $Ra_\omega=5\times10^3$, two well defined cylindrical formations spanning the z direction and nearly touching the walls emerge (as in the $Ra_\omega=1\times10^4$ case).

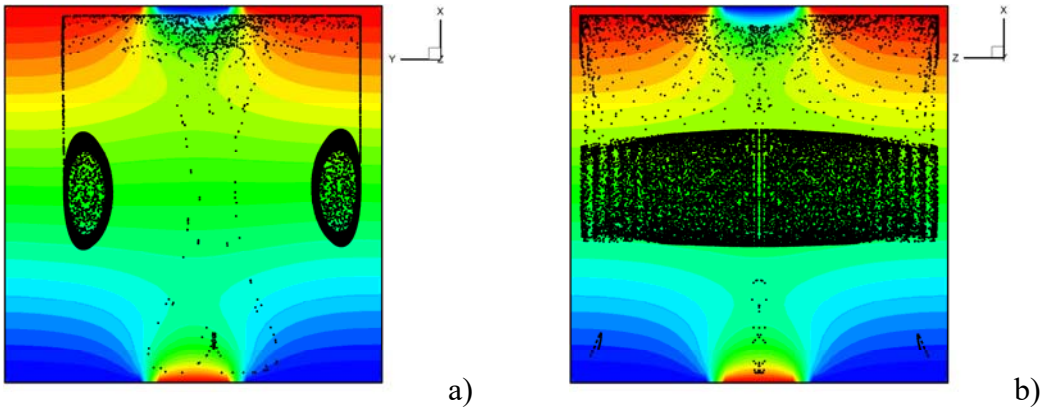

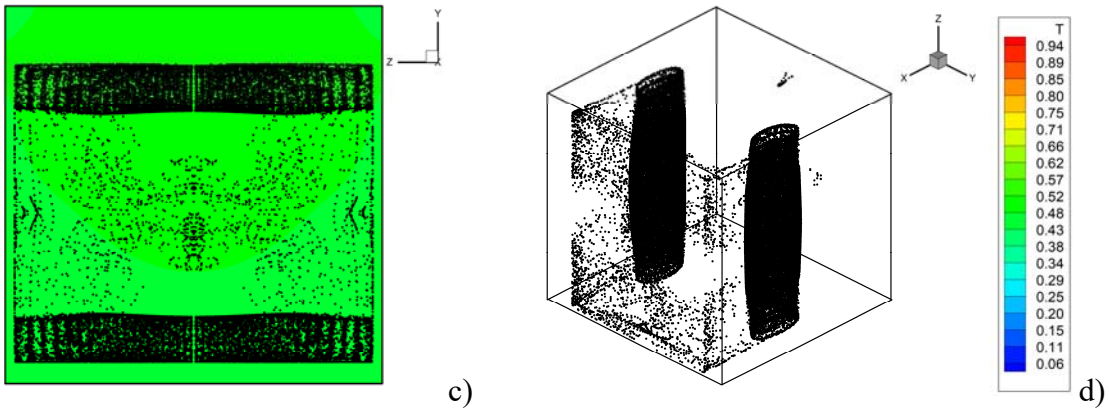

Figure 5: *Snapshot (3D views for t≅8.96) of particle structures and related temperature distribution for $\gamma=10^8$, $Ra_\omega=5\times10^3$, $\varpi=10^3$, $St=5\times10^{-6}$, $\xi=2$, $\phi=0°$ and $l_s=0.2$: a) perspective perpendicular to the xy mid-plane, b) perspective perpendicular to the xz mid-plane, c) perspective perpendicular to the yz plane, d) Isometric 3D view.*

Nevertheless, Figure 6 reveals that when Ra_ω is increased to 2.1×10^4, such structures undergo a significant compression along the z-axis (towards the center of the cavity). As evident in Figure 7, the extent of compression increases with Ra_ω.

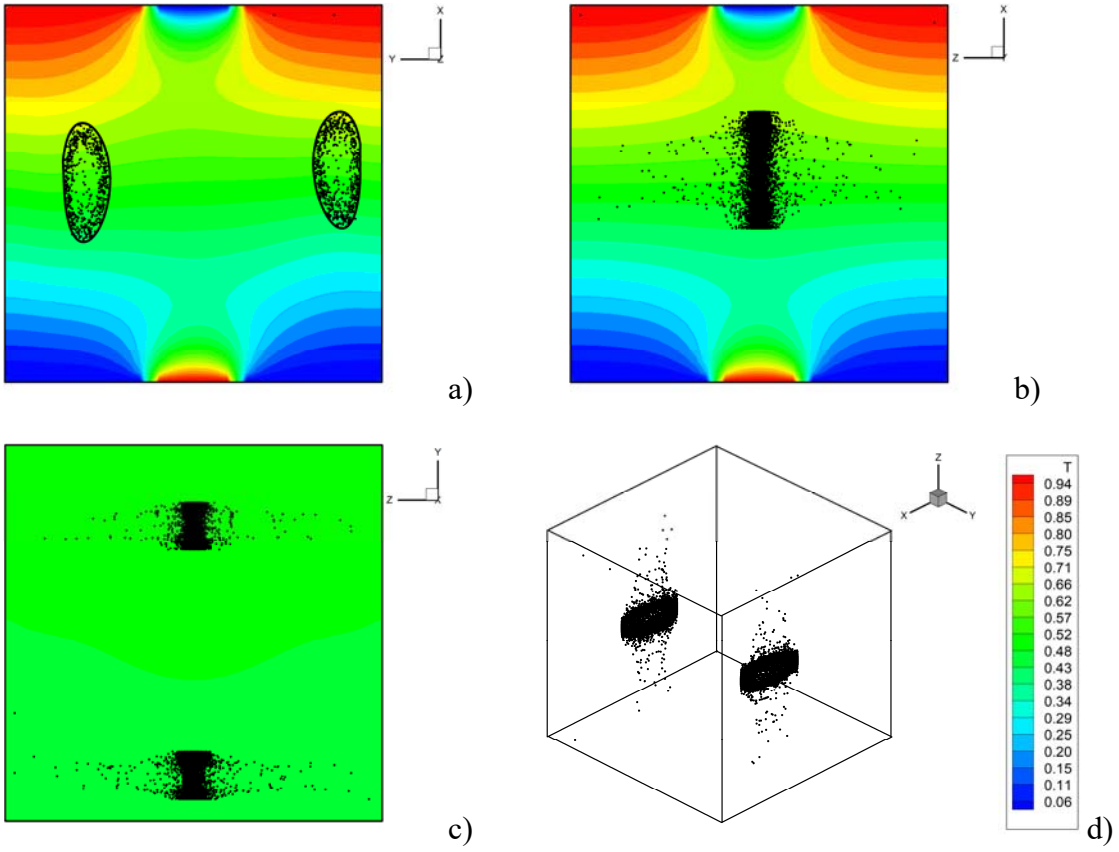

Figure 6: *Snapshot (3D views for t≅8.96) of particle structures and related temperature distribution for $\gamma=10^8$, $Ra_\omega=2.1\times10^4$, $\varpi=10^3$, $St=5\times10^{-6}$, $\xi=2$, $\phi=0°$ and $l_s=0.2$: a) perspective perpendicular to the xy mid-plane, b) perspective perpendicular to the xz mid-plane, c) perspective perpendicular to the yz plane, d) Isometric 3D view*

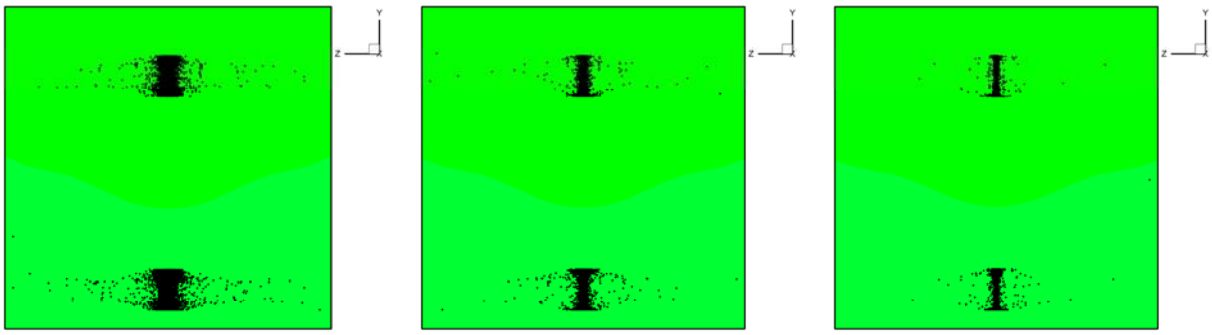

a) b) c)

Figure 7: *Snapshot (perspective view perpendicular to the yz plane) (3D views for t≅8.96) of particle structures and related temperature distribution for $\gamma=10^8$, $\varpi=10^3$, $St=5\times10^{-6}$, $\xi=2$, $\phi=0°$ and $l_s=0.2$: a) $Ra_\omega=2.1\times10^4$ b) $Ra_\omega=2.3\times10^4$ and c) $Ra_\omega=2.5\times10^4$*

4.3 Comparisons

The findings illustrated in the earlier sections are complemented here by plots that show quantitatively the variations experienced by the particle structures in terms of size. Figure 8a shows in detail the morphological evolution of the co-existing elongated and shallow structures for l_s =0.5 in terms of characteristic extensions along the z and y directions, respectively, as a function of Ra_ω. It can be seen that on increasing Ra_ω the elongated standard structures cease to exist as a given threshold is exceeded. Beyond such a threshold only the quadrupolar structures are possible.

For l_s =0.2, one of the observed key features is the axial compression of the cylindrical formations. The onset of this compression occurs at an earlier stage, and it causes a shrinkage in the x direction, as shown in Figure 8b. The corresponding y axis extension remains almost unaffected, that is, the diameter of these structures is nearly constant throughout the window of observations.

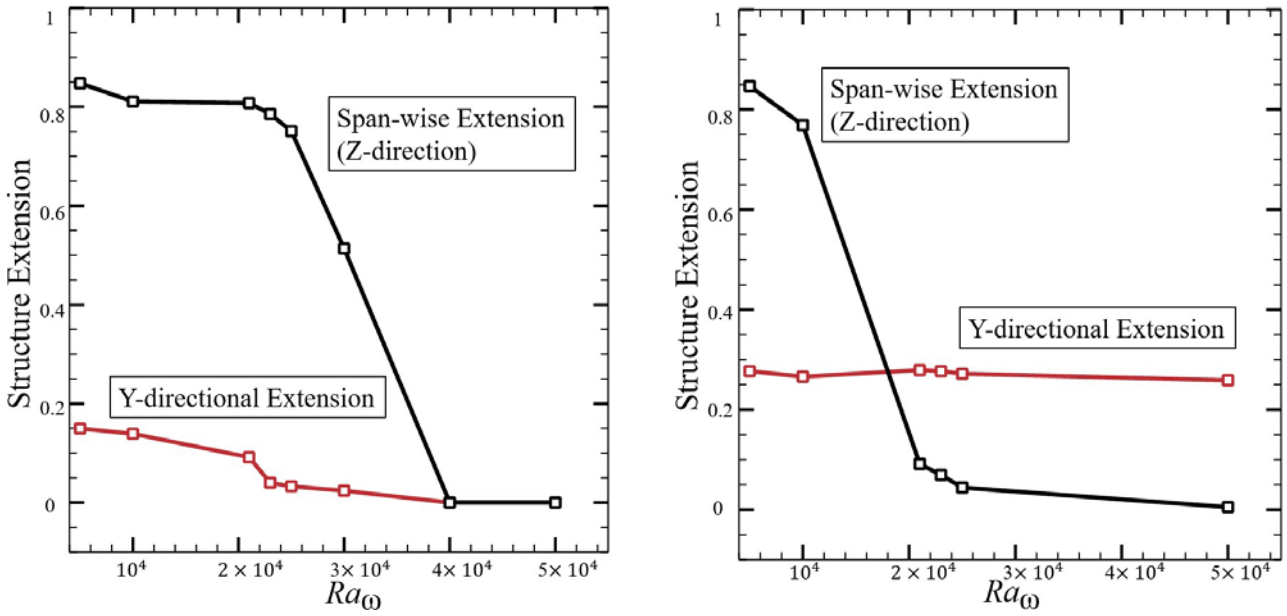

a) b)

Figure 8: *Morphological Evolution of Particle Accumulation Structures against Ra_ω a) l_s=0.5 b) l_s=0.2 .*

5. Conclusions

In an effort to expand the results of an existing line of inquiry, thermovibrational convection in a fluid containing dispersed inertial solid particles subjected to thermal inhomogeneities has been explored as a novel approach to control the morphology of particle accumulation structures in microgravity conditions. Two specific cases have been considered, namely, spot sizes l_s =0.2 and 0.5 as these were found to be the most intriguing and representative ones in an earlier numerical study. The value of the vibrational Rayleigh number has been changed to explore its effect on the existence of the particle structures and their typical size. On increasing Ra_ω, it has been found that for l_s = 0.5, for which previously two distinct coexisting patterns had been observed, each with individual multiplicity of 4, one of the two patterns is suppressed. As $Ra_\omega = 4\times10^4$ is exceeded, the shallow quadrupolar structure becomes dominant. Most interestingly, this indicates that when different attractors coexist in the physical domain, they may have different "attracting abilities" and that such abilities scale differently with the Rayleigh number (with one attractor replacing the other as the most attracting one as Ra_ω is varied in a certain range).

For l_s =0.2, an axial compression of the structures towards the center of the cavity along the z-direction is observed. This happens for $Ra_\omega = 2\times10^4$ and leads to a shrinkage of the structure length by a factor of 4, while its diameter remains nearly constant.

Together with the earlier studies, the present work contributes to the creation of a database of numerical results about the influence of thermal boundary conditions and strength of thermos-vibrational flow on the properties of the emerging particle structures. This extensive set of data will be used in the future to train an algorithm of artificial intelligence able to exploit the related inverse relationship, i.e. capable of providing the required thermal boundary conditions and values of the governing non-dimensional numbers for "given" (decided a priori) morphology, multiplicity and size of the particle structures.

Proposed changes/addition in the final manuscript:

1. The final manuscript shall discuss in further detail (pictorially and graphically) how and why the structures are compressed (as discussed) by comparing the velocity field data obtained from these simulations.

2. A novel post-processing technique (currently being worked on) is proposed, that quantifies the particle accumulation as a scalar parameter varying with time that considers local particle aggregation within the cells of the domain to estimate the overall 'strength' of the accumulation varying with time and cases being considered.

Acknowledgments

This work has been supported by the UK Space Agency (STFC grants ST/S006354/1, ST/V005588/1, ST/W002256/1 and ST/W007185/1) in the framework of the PARTICLE VIBRATION (T-PAOLA) project.

References

[1] Wei, C.;Wang, J.; He, Y.; Li, J.; Beaugnon, E. Solidification of Immiscible Alloys under High Magnetic Field: A Review. Metals 2021, 11, 525. https://doi.org/ 10.3390/met11030525
[2] Gui N., Li X., Tu X., (2016), "Progress of Particle Flow, Fluid/Solid Mechanics, and Heat Transfer in Advanced Gas/Water Nuclear Reactors", *Science and Technology of Nuclear Installations*, vol. 2016, Article ID 2512634, 2 pages, 2016. https://doi.org/10.1155/2016/2512634
[3] Li G., Gao J., Wen P., Zhao Q., Wang J., Yan J., Yamaji A., (2020), A review on MPS method developments and applications in nuclear engineering, Computer Methods in Applied Mechanics and Engineering, 367, 113166, ISSN 0045-7825, https://doi.org/10.1016/j.cma.2020.113166.
[4] Zong J. and Yue J., (2022), Continuous Solid Particle Flow in Microreactors for Efficient Chemical Conversion, *Industrial & Engineering Chemistry Research*, 61 (19), 6269-6291. DOI: 10.1021/acs.iecr.2c00473
[5] Rogers A.J., Hashemi A. and Ierapetritou M.G., (2013), Modeling of Particulate Processes for the Continuous Manufacture of Solid-Based Pharmaceutical Dosage Forms, *Processes*, 1, 67-127; doi:10.3390/pr1020067
[6] Rahmat, A., Barigou, M. and Alexiadis, A. (2020), "Numerical simulation of dissolution of solid particles in fluid flow using the SPH method", International Journal of Numerical Methods for Heat & Fluid Flow, Vol. 30 No. 1, pp. 290-307. https://doi.org/10.1108/HFF-05-2019-0437
[7] Sturtz C., Limare A., Tait S., Kaminski É., (2022), Birth and Decline of Magma Oceans in Planetesimals: 1. Experimental Study of Erosion and Deposition of Particles in an Internally Heated Convecting Fluid, *JGR Planets*, 127(12), https://doi.org/10.1029/2021JE007000
[8] Santhosh B.M. and Lappa M., (2023) On the relationship between solid particle attractors and thermal inhomogeneities in vibrationally driven fluid-particle systems. *Physics of Fluids* 1 October 2023; 35 (10): 103316. https://doi.org/10.1063/5.0170162
[9] Lappa M., (2019a), On the Nature of Fluid-dynamics, Chapter 1 (pp. 1-64) in Understanding the Nature of Science, Patrick Lindholm Editor, Nova Science Publishers Inc., Series: Science, Evolution and Creationism, BISAC: SCI034000, ISBN: 978-1-53616-016-1
[10] Lyubimov D. V., Lyubimova T. P., and Straube A. V., (2005), "Accumulation of solid particles in convective flows," *Microgravity Sci. Technol*. 16, 210–214.
[11] Sharifulin A.N., Plotnikov S.A., · Lyubimova T.P, (2022), Influence of the Directions of Vibrations and Gravity on the Formation of Vortex Structures of a Nonuniformly Heated Fluid in a Square Cavity, *Microgravity Science and Technology*, 34:97 (12 pages).
[12] Haller G. and Sapsis T., (2008), "Where do inertial particles go in fluid flows?," *Physica D* 237(5), 573–583.
[13] Sapsis T. and Haller G., (2010), Clustering criterion for inertial particles in two-dimensional time-periodic and three-dimensional steady flows, *Chaos*, 20, 017515.
[14] Lappa M., (2013), "On the variety of particle accumulation structures under the effect of g-jitters," *J. Fluid Mech*., 726, 160–195, doi: 10.1017/jfm.2013.203.
[15] Lappa M., (2014), "The patterning behavior and accumulation of spherical particles in a vibrated non-isothermal liquid," *Phys. Fluids*, 26(9), doi: 10.1063/1.4893078.
[16] Lappa M., (2017), "On the multiplicity and symmetry of particle attractors in confined non-isothermal fluids subjected to inclined vibrations," *Int. J. Multiph. Flow*, 93, 71–83, Jul. 2017, doi: 10.1016/j.ijmultiphaseflow.2017.03.015.
[17] Lappa M., (2019b), "On the formation and morphology of coherent particulate structures in non-isothermal enclosures subjected to rotating g-jitters," *Phys. Fluids*, 31(7), doi: 10.1063/1.5098438.
[18] Lappa M. and Burel T., (2020), "Symmetry breaking phenomena in thermovibrationally driven particle accumulation structures," *Phys. Fluids*, 32(5), doi: 10.1063/5.0007472.
[19] M. Lappa, (2024), "New In-Orbit Self-Assembly Principles And Manufacturing Techniques", Article In *"Why Space? The Opportunity For Material Science And Innovation",* A Publication Of UKRI_STFC And The Satellite Applications Catapult, Editors: M. Lappa. I. Hamerton, P.C.E. Roberts, A. Kao, M. Domingos, H. Soorghali. P. Carvil, Isbn: 9781914241680, Pp. 62-65].
[20] Lappa M. , (2022), "Characterization of two-way coupled thermovibrationally driven particle attractee," *Phys. Fluids*, 34(5), 053109 (27 pages), doi: 10.1063/5.0091520
[21] Crewdson G., Evans M., Lappa M., (2022), Two-dimensional vibrationally-driven solid particle structures in non-uniformly heated fluid containers, *Chaos*, 32(10) 103119 (13 pages).
[22] Crewdson G. and Lappa M., (2022), "An Investigation into the Behavior of Non-Isodense Particles in Chaotic Thermovibrational Flow," *Fluid Dyn. Mater. Process*., 18(3), 497–510, doi: 10.32604/fdmp.2022.020248

[23] Clift R., Grace J.R. and Weber M.E., Bubbles, drops, and particles. Courier Corporation, 2005, ISBN 0486317749, 9780486317748
[24] Gresho P.M., (1991), "Incompressible fluid dynamics: some fundamental formulation issues", *Ann. Rev Fluid Mech*., 23: 413-453.
[25] Ladyzhenskaya O.A., (1969), "The Mathematical Theory of Viscous Incompressible Flow", Gordon and Breach, 2nd Edition, New York - London, 1969.